SUPPLEMENTARY INFORMATION

Control of interlayer friction in two-dimensional ferromagnetic $CrBr_3$

Xinyue Bi [a], Yushu Xu [b], Xinqi Zhang [a], Junqin Shi [a], Tengfei Cao [a], Feng Zhou[a, c], Weimin Liu[a, c], Xiaoli Fan [a, *]

[a] State Key Laboratory of Solidification Processing, Center of Advanced Lubrication and Seal Materials, School of Material Science and Engineering, Northwestern Polytechnic University, Xi'an, Shaanxi 710072, China

[b] Queen Mary University of London Engineering School, Northwestern Polytechnical University, 127 YouYi Western Road, Xi'an, Shaanxi 710072, China

[c] State Key Laboratory of Solid Lubrication, Lanzhou Institute of Chemical Physics, Chinese Academy of Sciences, Lanzhou 730000, China

*Corresponding author: xlfan@nwpu.edu.cn

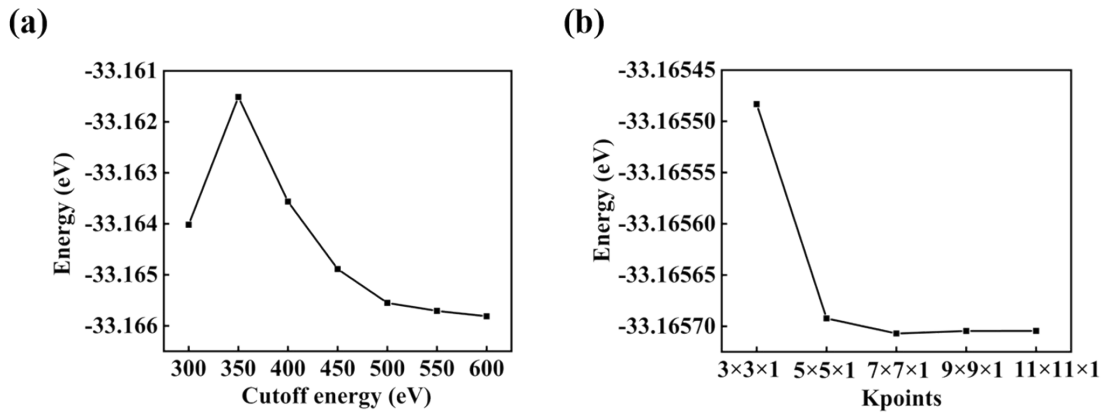

Figure S1. The total energy of monolayer $CrBr_3$ versus the (a) cutoff energy and (b) k point.

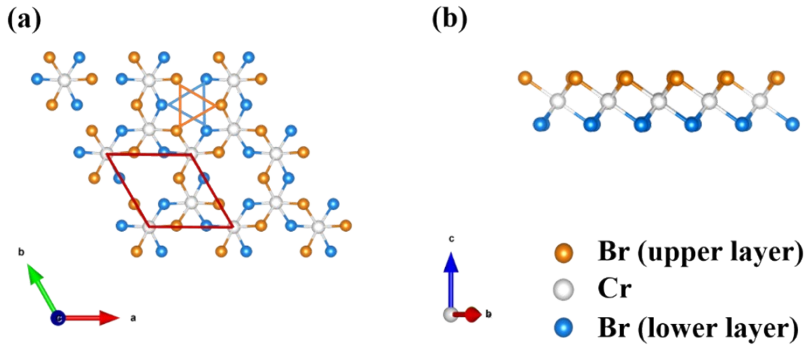

Figure S2. (a) Top and (b) side views of $CrBr_3$ monolayer. The rhombic regime represents the unit cell. White balls represent the Cr atoms; orange (blue) balls represent the Br atoms in the upper (lower) layer of $CrBr_3$. The Cr atoms are arranged in a honeycomb lattice and each Cr atom is surrounded by six Br atoms in an octahedron. The Br atoms in both the upper and lower layers are arranged in a triangle lattice. The equilateral triangles composed of the Br atoms in upper (lower) layer of $CrBr_3$ are highlighted in orange (blue) triangles.

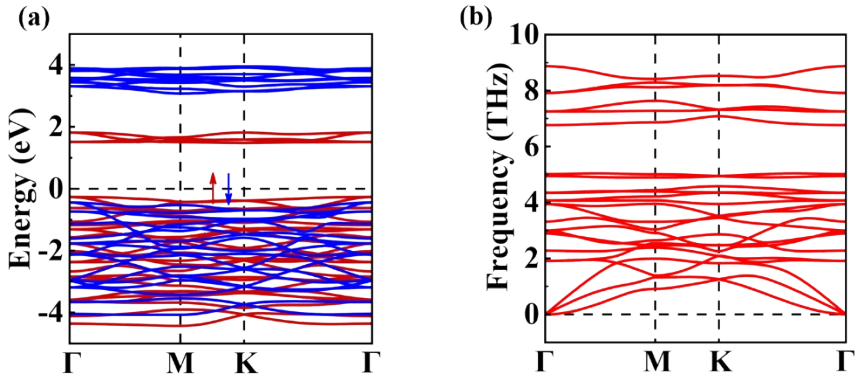

Figure S3. (a) Band structure and (b) phonon dispersion of $CrBr_3$ monolayer. The red (blue) lines represent the the spin-up (spin-down) states.

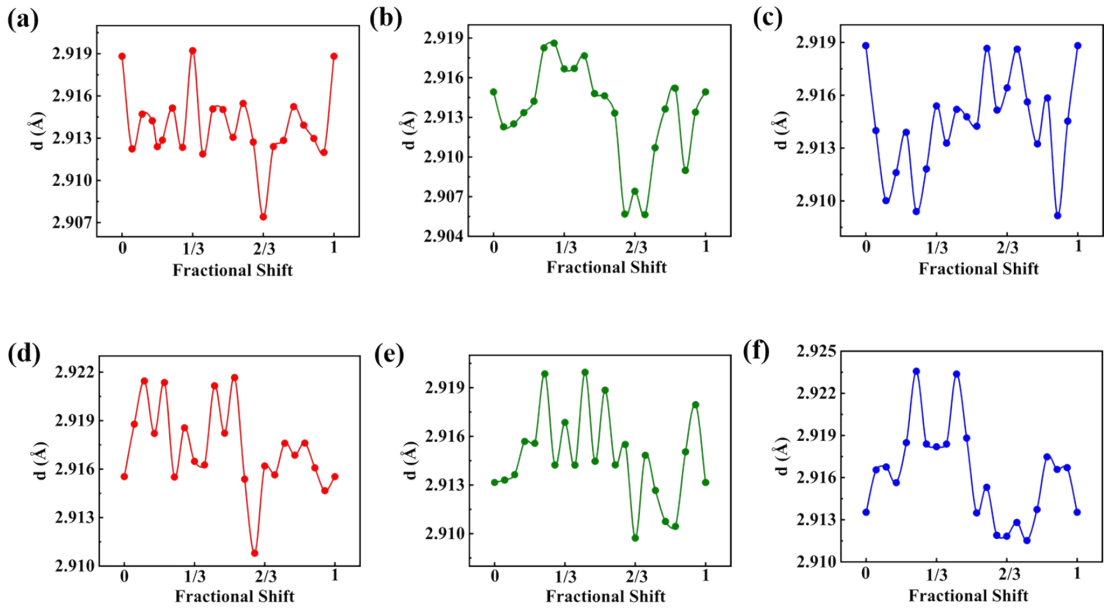

Figure S4. The variation of the interlayer distance (d) of R-type/H-type $CrBr_3$ bilayer along sliding path (a) R1, (b) R2, (c) R3 and (d) H1, (e) H2, (f) H3.

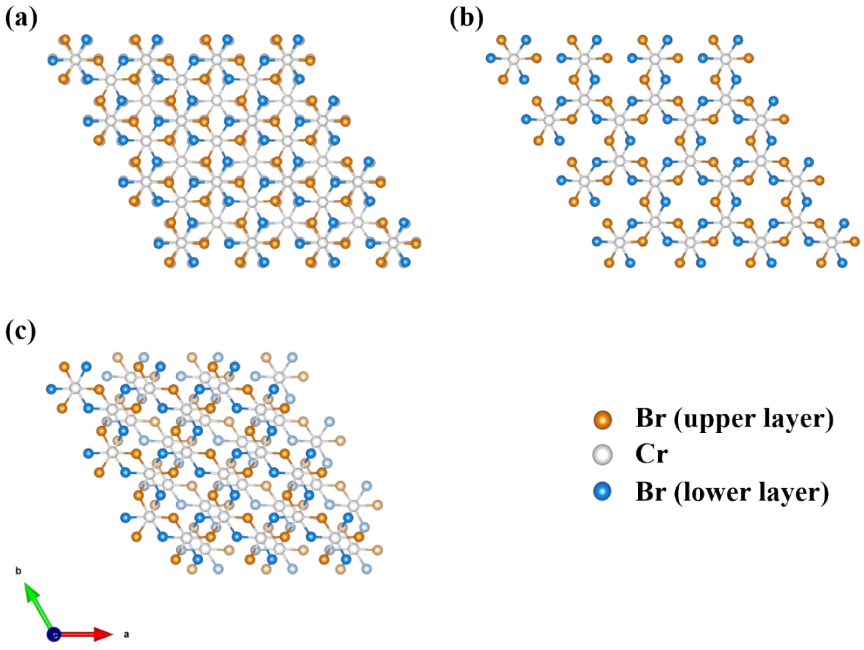

Figure S5. Top views for the atomic structure of R-type bilayer $CrBr_3$ in stacking configurations corresponding to (a) Hollow, (b) Top and (c) Bridge sites along the high symmetry sliding pathway R1. White balls represent the Cr atoms; orange (blue) balls represent the Br atoms in the upper (lower) layer of $CrBr_3$. The transparency of atoms in the bottom $CrBr_3$ of the three stacking configurations are adjusted higher to be clear.

Table S1. The calculated interlayer binding energies of the lowest energy configurations

for R-type and H-type bilayer $CrBr_3$ in ferromagnetic (FM) and antiferromagnetic (AFM) configurations.

	Binding energy (meV/atom)	
	FM	AFM
R-type	-60.25	-59.63
H-type	-59.25	-58.84

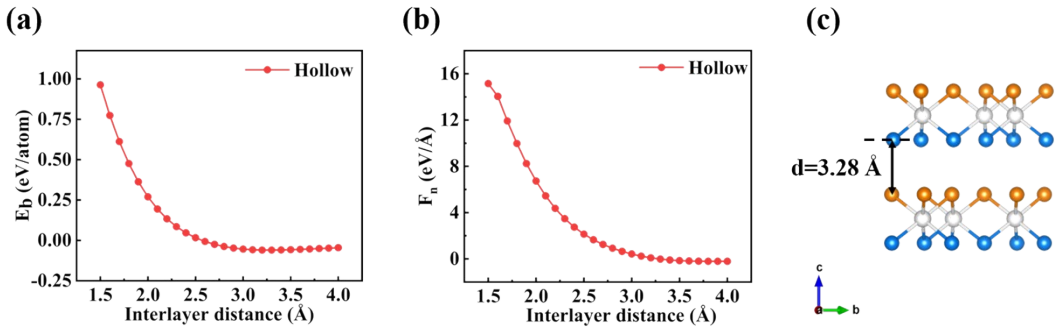

Figure S6. The variation of (a) binding energy (E_b) and (b) normal load (F_n) of the stacking configuration corresponding to the Hollow site in its ground state FM along the high symmetry sliding pathway R1 with respect to the interlayer distance. (c) The interlayer distance (d) of the Hollow configuration.

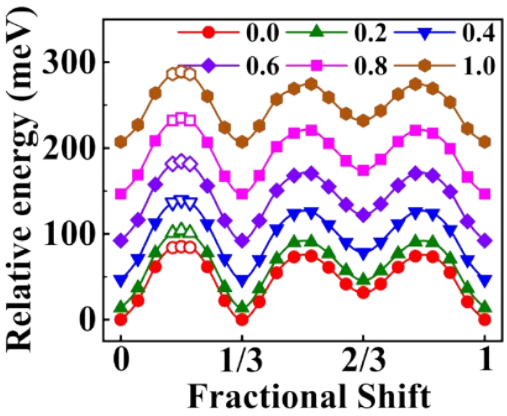

Figure S7. Energy profiles of the R-type bilayer $CrBr_3$ with the top $CrBr_3$ sliding over the bottom one along the high symmetry sliding pathway R1 under the normal load of 0.0, 0.2, 0.4, 0.6, 0.8 and 1.0 eV/Å. The starting points are chosen as the stacking structure with the minimum energy, and the minimum energy value along path R1 without normal load is set to zero. The solid and hollow shapes indicate the stacking

configurations being ferromagnetic (FM) and antiferromagnetic (AFM), respectively.

Detailed method for realizing carrier doping:

Carrier doping is realized by changing the parameter “NELECT”, which represents the number of the electrons. The value of “NELECT” greater/less than the total number of valence electrons means charge/hole doping.

Method used for calculating the contribution of electrostatic interactions to the total energy:

The energy calculated without vdW-dispersion energy-correction is regarded as the contribution of electrostatic interactions to the total energy.